Available online at www.sciencedirect.com
SCIENCE DIRECT
Journal of Power Sources 145 (2005) 644–651
JOURNAL OF POWER SOURCES
www.elsevier.com/locate/jpowsour

$WO_3/CeO_2/YSZ$ nanocomposite as a potential catalyst for methanol reforming

Marta Maria Natile*, Antonella Glisenti

Dipartimento di Scienze Chimiche, Università di Padova, via F. Marzolo, 1-35131 Padova, Italy

Accepted 28 January 2005
Available online 13 June 2005

Abstract

A $WO_3/CeO_2/YSZ$ nanocomposite material [W/Zr nominal atomic ratio = 0.025, Ce/Zr nominal atomic ratio = 0.020] was prepared by wet impregnation and characterized by means of X-ray photoelectron and diffuse reflectance infrared Fourier transform spectroscopic techniques, X-ray diffraction and thermal analysis.

Both tungsten and cerium oxides are significantly reduced at the interface with YSZ: Ce(III), in particular, seems to be the prevailing species.

The interaction of the $WO_3/CeO_2/YSZ$ nanopowder with pyridine and CO_2 allowed to investigate the acidic/basic sites. Weak contributions at 1602, 1625 and 1647 cm^{-1} suggest the presence of Lewis and Brønsted acidic sites, whereas basic sites are not evidenced by the interaction with carbon dioxide. The presence of tungsten oxide causes the decrement of the acidic/basic sites, as indicated by the comparison with the results obtained on the CeO_2/YSZ support. Consistently, the interaction with methanol is mainly molecular.

The oxidation of methanol was investigated both in the absence and in the presence of water. In the last case carbon dioxide starts forming from room temperature.

Keywords: Nanocomposite oxide-based catalyst; Methanol; Tungsten oxide; Cerium oxide; Yttria-stabilized zirconia

1. Introduction

In recent years, the interest in clean and efficient energy sources is growing significantly. The two-folds objective of promoting economic competitiveness and environmental sustainability guides the research in the development of advanced and clean energy technologies. Among the various recently developed devices, fuel cells (FCs) are the most promising thanks to their high efficiencies [1,2].

Solid oxide fuel cells (SOFCs), in particular, show a great deal of advantages such as fuel flexibility and higher stability; moreover, SOFCs do not encounter problems with slow oxygen reduction kinetics [3].

In this paper we focus our attention on nanocomposite oxide-based systems to be used as active materials in anodes. Nanocomposite materials offer great possibilities. An appropriate preparation procedure allows to deposit nanodimensioned oxide particles taking thus advantage of the reactivity of nanoclusters [4]. Moreover, an active oxide can be used as a support.

A $WO_3/CeO_2/YSZ$ sample was prepared depositing (by means of wet impregnation) CeO_2 and WO_3 nanoclusters on a commercial YSZ (this material is commonly used in SOFC). The obtained powder was characterized by means of X-ray diffraction (XRD), thermal analysis (TGA) as well as X-ray photoelectron (XPS) and diffuse reflectance infrared Fourier transform (DRIFT) spectroscopic techniques.

Both cerium and tungsten oxides can play an important role in oxidation reactions. Cerium oxide is a mixed conductor exhibiting both ionic and electronic conductivity (n-type); the accessibility of (IV) and (III) oxidation states enhances its catalytic activity [5]. Tungsten oxide is known to be an active catalyst for olefin oxidation [6–8], however, the substoichiometric tungsten oxides (such as $WO_{2.95}$, $WO_{2.90}$ and $WO_{2.75}$) show more selectivity than WO_3. This behav-

* Corresponding author. Tel.: +39 049 8275196; fax: +39 049 8275161.
E-mail address: martamaria.natile@unipd.it (M.M. Natile).

0378-7753/$ – see front matter © 2005 Elsevier B.V. All rights reserved.
doi:10.1016/j.jpowsour.2005.01.084

ior is discussed in terms of a mechanism involving the W(V) and/or W(IV) ions as well as the different crystalline structure of the substoichiometric oxides with respect to WO_3 and the presence of crystallographic shear planes [6,7].

The active sites distributed on the sample surfaces were investigated by means of probe molecules (pyridine and carbon dioxide) and compared with those observed on WO_3 [9] and CeO_2/YSZ [10].

IR spectroscopy can readily distinguish pyridine coordinated with Lewis acidic sites from pyridinium ions originated by the interaction between pyridine and the Brønsted acidic sites [11–14]. Pyridine H-bound to the surface can also be distinguished. Different species can derive from the interaction of carbon dioxide with the acidic/basic surface sites. The adsorption on hydroxyl groups gives rise to bicarbonate species, whereas the interaction with Lewis acidic sites causes the formation of carbonyl (because of the presence of an oxygen vacancy) or carboxyl groups. The adsorption on basic sites (coordinatively unsaturated oxygen anions) originates unidentate carbonates, whereas the interaction with an acidic metal ion and its neighboring basic oxygen originates bidentate carbonates [15–18].

The information concerning active sites was used to better understanding the interaction between methanol and the WO_3/CeO_2/YSZ surface. Methanol is an important probe molecule as well as an interesting combustible for fuel cells [2]. In this paper we investigated the reactivity of the nanocomposite with respect to methanol oxidation both in the absence and in the presence of water to take into consideration the steam reforming reaction. The interaction of methanol with the support (CeO_2/YSZ) and the pure oxides (WO_3, CeO_2, YSZ) was already investigated and will be considered for comparison [10,19].

2. Experimental

2.1. Catalyst preparation

The CeO_2/YSZ support was prepared by impregnating commercial yttria (8 mol%) stabilized zirconia (TOSOH, TZ-8Y) with an aqueous solution of $Ce(NO_3)_3{\cdot}6H_2O$ (Strem Chemicals, 99.9%) as indicated elsewhere [10]. The supporting powder was investigated by means of XP, DRIFT spectroscopic techniques and thermal analysis before the deposition procedure.

The WO_3/CeO_2/YSZ nanocomposite was obtained by wet impregnation of the described CeO_2/YSZ support with an aqueous solution of ammonium metatungstate, $(NH_4)_6(W_{12}O_{39}){\cdot}H_2O$ (Aldrich) [W/Zr nominal atomic ratio = 0.025, Ce/Zr nominal atomic ratio = 0.020] [20]. The obtained suspension was maintained under stirring for 2 days and then kept in rest for 1 day. Water was evaporated (in air) at 350 K and the obtained solid was treated at 773 K for 5 h (in air).

2.2. Reaction conditions and DRIFT measurements

The IR spectra were collected in a Bruker IFS 66 spectrometer (accumulating 128 scans) and displayed in the Kubelka–Munk units [21,22]. The resolution of the spectra was 4 cm^{-1}. The temperature of the powder has been checked by means of a thermocouple inserted into the sample holder directly in contact with the powder.

Prior to each experiment, ca. 50 mg of the sample were loaded in the sample cup of a low temperature reaction chamber (CHC) installed in the Praying Mantis™ accessory for diffuse reflection spectroscopy (Harrick Scientific Corporation) and fitted with ZnSe windows; the powder was kept in nitrogen flow to eliminate residual water until a stable IR spectrum was obtained (ca. 2 h). Then, the sample was exposed to the reactive species at a flow rate of 100–150 $cm^3\ min^{-1}$ before measurement. The spectrum of the clean surface was used as background.

The CHC chamber was filled with the pyridine or the alcohol vapors flowing nitrogen through a bubbler containing the liquid. In the case of exposure to a methanol + water mixture the liquid was a solution (1:1) of water (distilled) and methanol. The exposure to CO_2 (Air Liquide, 99.998%) was carried out connecting the gas outlet directly to the reaction chamber. Pyridine and methanol used for the chemisorption were taken from a commercial source (Sigma–Aldrich, spectroscopic grade) and used without further purification.

2.3. XPS measurements

XP spectra were recorded using a Perkin-Elmer PHI 5600 ci spectrometer with a standard Al Kα source (1486.6 eV) working at 350 W. The working pressure was less than 1×10^{-8} Pa. The spectrometer was calibrated by assuming the binding energy (BE) of the Au $4f_{7/2}$ line to lie at 84.0 eV with respect to the Fermi level. Extended spectra (surveys) were collected in the range 0–1350 eV (187.85 eV pass energy, 0.4 eV step, 0.05 s $step^{-1}$). Detailed spectra were recorded for the following regions: C 1s, O 1s, Zr 3d, Y 3d, Ce 3d and W 4f (11.75 eV pass energy, 0.1 eV step, 0.1 s $step^{-1}$). The standard deviation in the BE values of the XPS line is 0.10 eV. The atomic percentage, after a Shirley type background subtraction [23], was evaluated using the PHI sensitivity factors [24]. To take into consideration charging problems the C 1s peak at 285.0 eV was considered and the peaks BE differences were evaluated.

The sample for the XPS analysis was processed as a pellet by pressing the catalyst powder at ca. 7×10^6 Pa for 10 min; the pellet was then evacuated for 12 h at ca. 1×10^3 Pa.

2.4. Thermal analysis and XRD

Thermogravimetric analysis (TGA) and differential scanning calorimetry (DSC) were carried out in a controlled atmosphere using the simultaneous differential techniques (SDTs) 2960 of TA Instruments. Thermograms were recorded at

Table 1
XP peak positions (binding energy, eV) obtained for the $WO_3/CeO_2/YSZ$ nanocomposite; the corresponding values obtained for the pure oxide and the CeO_2/YSZ support are also reported.

Peaks	$WO_3/CeO_2/YSZ$	CeO_2/YSZ [10]	YSZ [10]	CeO_2 (523 K) [10]	WO_3 [9]
Zr $3d_{5/2}$	182.2	182.0	182.2		
Zr $3d_{3/2}$	184.6	184.4	184.6		
Y $3d_{5/2}$	157.1	157.1	157.3		
Y $3d_{3/2}$	159.1	159.0	159.1		
Ce $3d_{5/2}$					
V	882.7	882.5		882.9	
V′	886.1	885.8			
V″		889.0		889.0	
V‴		898.9		898.7	
Ce $3d_{3/2}$					
U		901.1		900.8	
U′	904.7	904.3			
U″		907.3		907.4	
U‴	916.8	916.9		916.8	
W $4f_{7/2}$	35.6				35.6
W $4f_{5/2}$	37.6				37.7
O 1s	530.7	529.8	530.1	529.6	530.6

5 K min^{-1} heating rates in air and in nitrogen flow. The temperature ranged from room temperature (RT) to 1273 K.

XRD patterns were obtained with a Bruker D8 Advance diffractometer with Bragg–Brentano geometry using a Cu Kα radiation (40 kV, 40 mA, λ = 0.154 nm).

3. Results and discussion

3.1. $WO_3/CeO_2/YSZ$ characterization

The XP data of the following systems $WO_3/CeO_2/YSZ$, CeO_2/YSZ, YSZ, CeO_2, WO_3 are compared in Table 1.

The Ce 3d XP spectrum obtained for the $WO_3/CeO_2/YSZ$ is compared with the corresponding signal recorded for CeO_2/YSZ and CeO_2 in Fig. 1. The Ce 3d peak positions (Table 1) and shape suggest the presence of Ce(III): the signals characteristic of Ce(III), *V′* and *U′*, are well evident [25,26]. The presence of Ce(III) becomes more and more evident when going from CeO_2 (heated at 523 K) to the supporting CeO_2/YSZ (heated at 523 K) to the $WO_3/CeO_2/YSZ$ sample (heated at 773 K). The reduction phenomenon can thus be attributed both to the higher calcination temperature and to the deposition procedure. By comparing the less evident presence of Ce(III) in the WO_3/CeO_2 treated at 773 K [10] and in the CeO_2/YSZ samples with the Ce(III) in the $WO_3/CeO_2/YSZ$ sample it can be concluded that the reduction has to be attributed also to the small dimensions of CeO_2 particles and consequently to their higher reactivity [27].

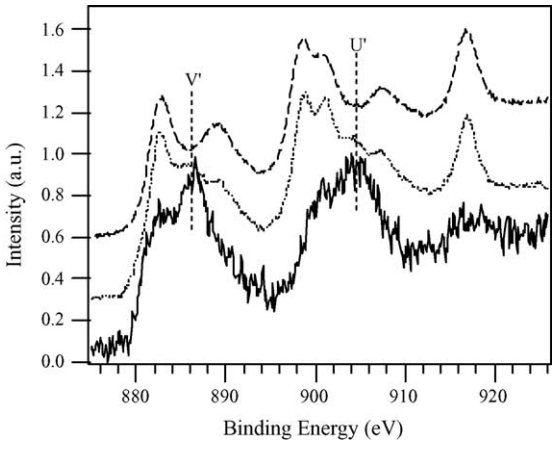

Fig. 1. Ce 3d spectrum obtained on the (—) $WO_3/CeO_2/YSZ$ nanocomposite compared with the corresponding spectra of (· · ·) CeO_2/YSZ and (- - -) CeO_2. (The spectra are normalized with respect to their maximum value).

The position of the two contributions of Zr 3d XP peak (Zr $3d_{5/2}$ and $3d_{3/2}$ peaks, respectively, at 182.2 and 184.6 eV, Fig. 2) and of the ones of Y 3d (Y $3d_{5/2}$ and $3d_{3/2}$ peaks, respectively, at 157.1 and 159.1 eV, Fig. 2) agrees with the expected values for YSZ (Table 1). The Zr 3d and Y 3d signals were observed at slightly lower BE in the CeO_2/YSZ samples [10]. The W $4f_{7/2}$ and $4f_{5/2}$ peak positions (35.6 and 37.6 eV, respectively, Fig. 3) are consistent with the presence of W(VI) in WO_3 (Table 1). The broadening of the signal toward the low BE side suggests the possible reduction of the tungsten cations.

The position of the O 1s XP peak (530.7 eV, Fig. 4) is almost identical to the value observed for WO_3 (530.6 eV) [9]. As evidenced in Fig. 4, the widening at the low BE side is in agreement with the peak positions in CeO_2 and YSZ (Table 1).

The XP atomic compositions of the sample ($WO_3/CeO_2/YSZ$) and the support (CeO_2/YSZ) are compared in Table 2. Consistently with the surface specific character of XPS [28,29], the obtained W/Zr and Ce/Zr atomic ratios are always higher than the corresponding nominal values. This allows to exclude the diffusion of the deposited oxide inside the support.

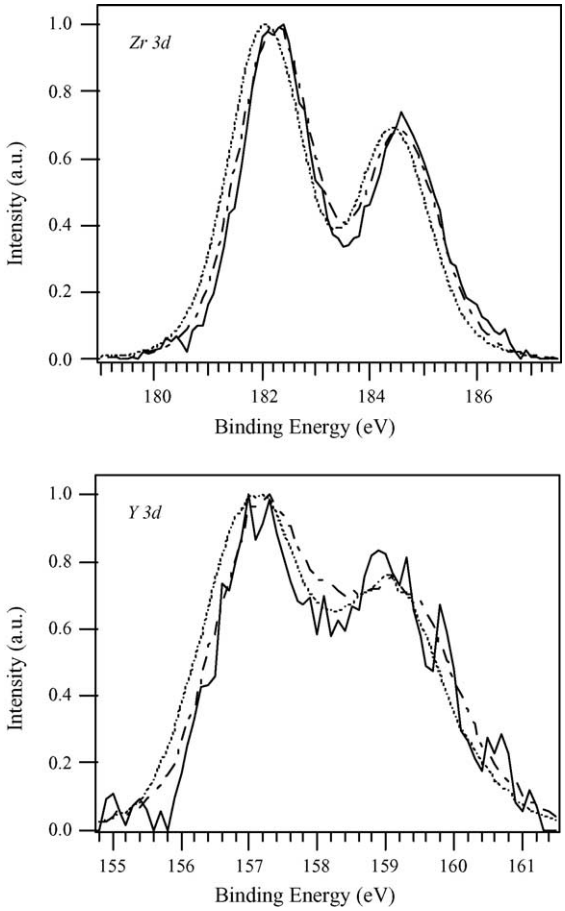

Fig. 2. Zr 3d and Y 3d XP spectra obtained on the (—) $WO_3/CeO_2/YSZ$ nanocomposite compared with the corresponding spectra of (···) CeO_2/YSZ and (-··-) YSZ. (The spectra are normalized with respect to their maximum value).

The XRD pattern of the $WO_3/CeO_2/YSZ$ sample coincides with that of the YSZ (Fig. 5): no diffraction peaks due to crystalline WO_3 or CeO_2 are observed. This demonstrates that the deposited cerium and tungsten oxides exist as highly dispersed or amorphous species [30].

The DRIFT spectra obtained as a function of temperature are reported in Fig. 6. The presence of molecularly chemisorbed water is suggested by the corresponding bending (1626 cm^{-1}) and stretching (broad signal around 3300 cm^{-1}) signals. H-bound and three-coordinated hydroxyl groups (around 3400–3500 cm^{-1}) also contribute to the broad band. At $T \geq 473$ K a broad and weak band between 3000 and 3600 cm^{-1} is still evident suggesting the presence of water molecules tightly interacting with

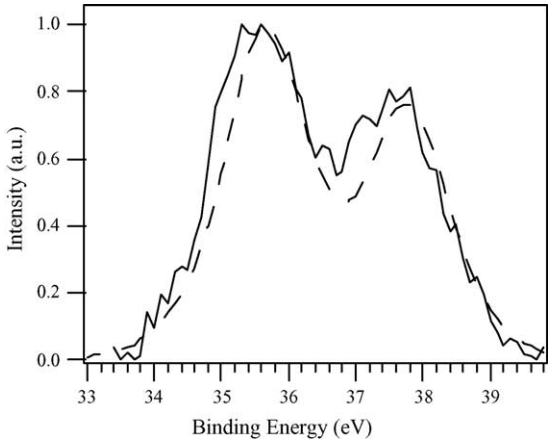

Fig. 3. W 4f spectrum obtained on the (—) $WO_3/CeO_2/YSZ$ nanocomposite compared with the corresponding spectrum of (––) WO_3. (The spectra are normalized with respect to their maximum value).

Lewis acidic sites. The shape and the behavior as a function of temperature of the O–H stretching band observed for $WO_3/CeO_2/YSZ$ and CeO_2/YSZ [10] systems are very similar: molecularly adsorbed water is the main adspecies. Some differences, however, are pointed out by the thermal analysis.

The thermogravimetric (TG) spectra of the $WO_3/CeO_2/YSZ$, of the support (CeO_2/YSZ) and of the pure oxides are compared in Fig. 7. The investigation of TG spectrum of $WO_3/CeO_2/YSZ$ reveals a weak and continuous weight loss between RT and about 900 K. Moreover, the weight loss is lower than that observed on the supporting CeO_2/YSZ. This

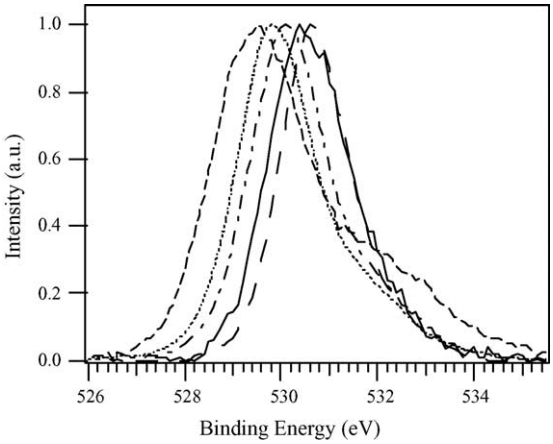

Fig. 4. O 1s XP spectrum obtained on the (—) $WO_3/CeO_2/YSZ$ nanocomposite compared with the corresponding spectra of (- - -) CeO_2, (-··-) YSZ, (···) CeO_2/YSZ and (––) WO_3. (The spectra are normalized with respect to their maximum value).

Table 2
Comparison between the nominal and XP atomic ratios of the sample ($WO_3/CeO_2/YSZ$) and of the support (CeO_2/YSZ)

Samples	XPS				Nominal	
	Ce 3d/Zr 3d	W 4f/Ce 3d	W 4f/Zr 3d	O/(W 4f + Ce 3d + Zr 3d + Y 3d)	Ce/Zr	W/Zr
$WO_3/CeO_2/YSZ$	0.66	0.28	0.18	2.43	0.020	0.025
CeO_2/YSZ	0.31	–	–	–	0.020	–

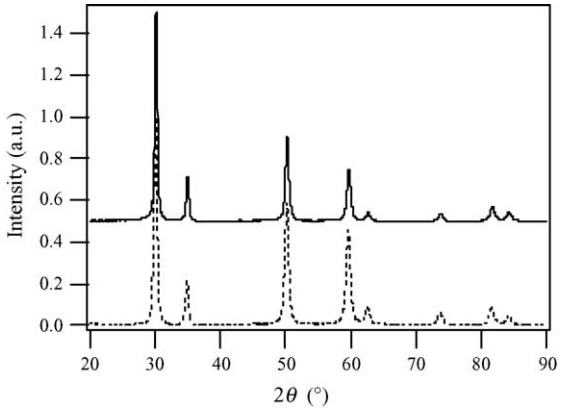

Fig. 5. XRD patterns of the (—) $WO_3/CeO_2/YSZ$ nanocomposite and of the (···) YSZ.

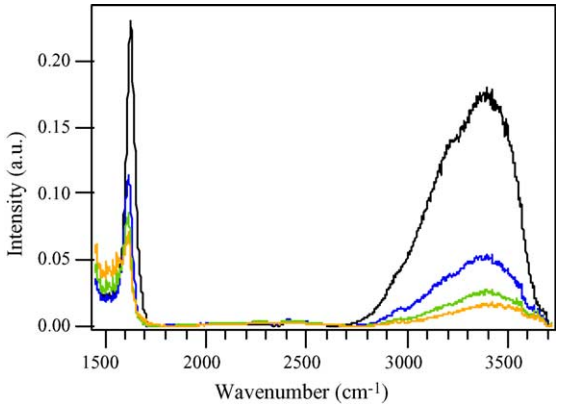

Fig. 6. DRIFT spectra of the $WO_3/CeO_2/YSZ$ nanocomposite obtained at different temperatures: (—) RT, (—) 373 K, (—) 423 K and (—) 473 K.

suggests a lower hydroxylation, in agreement with the XP and IR data. The comparison with the TG spectrum of WO_3 confirms the role of this oxide in the hydroxylation decrease. The lower hydroxylation of $WO_3/CeO_2/YSZ$ with respect to CeO_2/YSZ could indicate the grafting of WO_3 to the support by a condensation of hydroxyl groups.

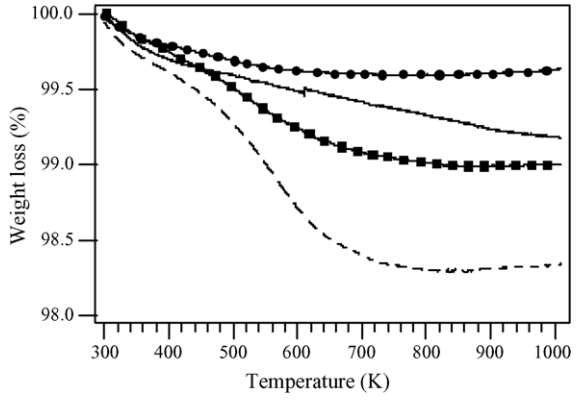

Fig. 7. TG spectrum of the (—) $WO_3/CeO_2/YSZ$ nanocomposite compared with the corresponding spectra of (- - -) CeO_2/YSZ, (■) YSZ and (●) WO_3.

No signals characteristic of carbonate species are observed in the IR spectral region characteristic of O–C–O stretching vibrations. This is an important result considering that the formation of carbonate species was observed on the WO_3/CeO_2 and on the CeO_2/YSZ systems and on the ceria [10]. Such phenomenon, in fact, is correlated with the strong tendency of lanthanide oxides toward atmospheric carbon dioxide adsorption and formation of stable surface carbonates [31]. Inactivity of $WO_3/CeO_2/YSZ$ with respect to atmospheric carbon dioxide is interesting because carbonate species can poison the active sites and thus influence the reactivity.

3.2. Interaction with pyridine and carbon dioxide

The DRIFT spectrum obtained after exposure to pyridine is shown in Fig. 8. The spectrum shows several contributions suggesting the presence of liquid-like and H-bound pyridine (1441, 1578 and 1597 cm^{-1}, Fig. 8a and b) [32–35]. Similar signals were observed upon exposing a reduced ceria powder to pyridine [10].

Two signals at 1489 and 1625 cm^{-1} (Fig. 8a and b) indicate the presence of pyridine interacting with strong Lewis acidic sites, whereas a contribution around 1539 cm^{-1} agrees with pyridine bound to Brønsted acidic sites.

The evacuation with N_2 rapidly removes liquid-like and H-bound pyridine revealing a new signal at 1602 cm^{-1} characteristic of pyridine coordinated to rather weak Lewis acidic sites. A small peak at about 1647 cm^{-1}, ascribable to pyridine interacting with Brønsted acidic sites [14], grows with evacuation time.

The exposure to pyridine deeply modifies the O–H stretching region: new signals appear between 3100 and 3550 cm^{-1} and between 3600 and 3750 cm^{-1} (Fig. 8c) suggesting a significant interaction.

The comparison with the results obtained for the supporting CeO_2/YSZ clearly indicates a change in the acidic sites as a consequence of the deposition of tungsten oxide. In fact, pyridine interacted quantitatively with the supporting surface giving rise to two peaks at 1616 and 1647 cm^{-1} [10]. Moreover, WO_3 is known to be an acidic catalyst: several signals (1608, 1614, 1625, 1643 and 1660 cm^{-1}) were observed on its surface after exposure to pyridine [9].

DRIFT spectrum collected after the exposure of $WO_3/CeO_2/YSZ$ to CO_2 does not indicate the presence of basic sites: the formation of carbonate species is not observed. Moreover, all the signals characteristic of CO_2 disappear after evacuation; this result indicates that CO_2 does not interact with the $WO_3/CeO_2/YSZ$ surface. A similar result was observed on WO_3 [9], whereas the acidic and basic reactive sites distributed on the surface of CeO_2/YSZ are responsible for the formation of carbonate species as a consequence of the interaction with carbon dioxide [10].

Summarizing, the deposition of WO_3 on the CeO_2/YSZ surface seems to cause a certain decrease of the acidic and

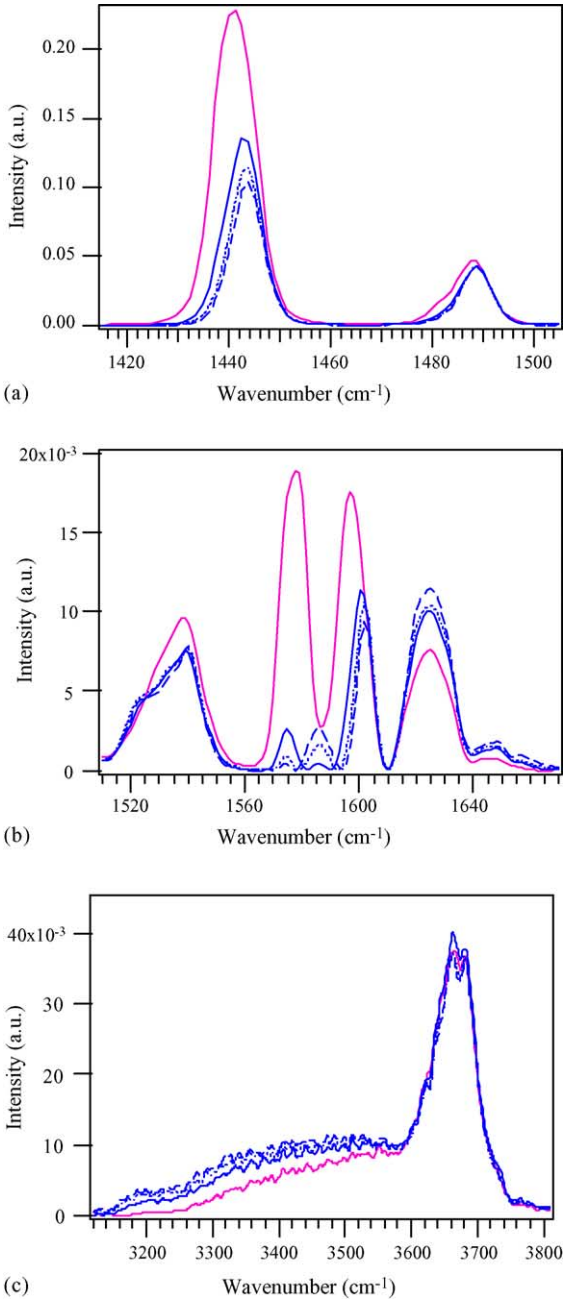

Fig. 8. DRIFT spectra obtained after exposing (at RT) the $WO_3/CeO_2/YSZ$ nanocomposite to the pyridine + N_2 mixture (——) and then to the nitrogen flow for 5 min (——), 30 min (·····) and 60 min (- - - -); (a) spectral region from 1415 to 1505 cm^{-1}; (b) spectral region from 1510 to 1670 cm^{-1}; (c) spectral region from 3120 to 3810 cm^{-1}.

basic sites. This is rather surprising because several acidic sites were observed on the WO_3 surface [9].

3.3. Interaction with methanol

The reactivity of the nanocomposite was investigated both with respect to methanol and to a methanol + water mixture.

The interaction of the $WO_3/CeO_2/YSZ$ with methanol and methanol + water is mainly molecular, as evidenced by the

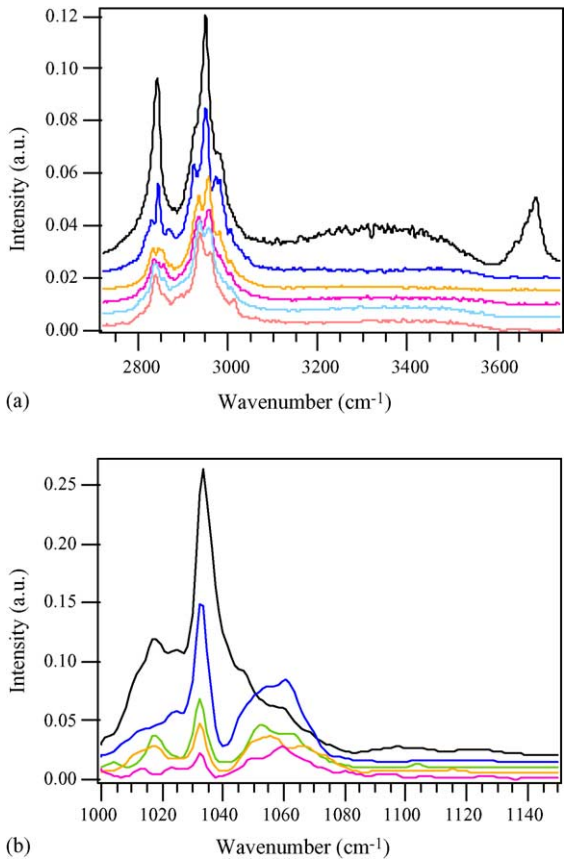

Fig. 9. DRIFT spectra obtained after exposing the $WO_3/CeO_2/YSZ$ nanocomposite to a methanol + water mixture at different temperatures: (—) RT, (——) 373 K, (——) 473 K, (——) 523 K, (——) 573 K and (——) 603 K; (a) spectral region from 2720 to 3740 cm^{-1}; (b) spectral region from 1000 to 1150 cm^{-1}.

broad band at about 3350 cm^{-1} (Fig. 9a). Gas phase methanol [36,37] dominates both the C–O (1013, 1032 and 1052 cm^{-1}) and the C–H (2843 and 2949 cm^{-1}) stretching regions of the IR spectrum obtained after exposure to methanol at RT (Fig. 9a and b). In the C–O stretching region weak contributions (at 1018, 1023, 1047 and 1059 cm^{-1}) [38,39] suggest a certain dissociative interaction.

Dissociative interaction is slightly more evident (both in the presence and in the absence of water) at higher temperatures, as indicated by the increasing intensity of the signals due to the C–O stretching and of the peaks at 2838 and 2924 cm^{-1} attributed to the symmetric and asymmetric C–H stretching of methoxy groups (Fig. 9a and b) [38,39]. The N_2 flow easily removes the adsorbed species.

It is noteworthy observing that the only revealed oxidation product is carbon dioxide, evidenced by the broad band between 2250 and 2400 cm^{-1} (Fig. 10a and b). CO_2 forms at RT in presence of water and at $T \geq 573$ K when water is absent. Because of the absence of reactive sites (as already discussed) carbon dioxide is completely removed by N_2.

It is interesting to compare the behavior of the $WO_3/CeO_2/YSZ$ nanocomposite and related systems. Methanol interacts dissociatively with the support (CeO_2/YSZ) and

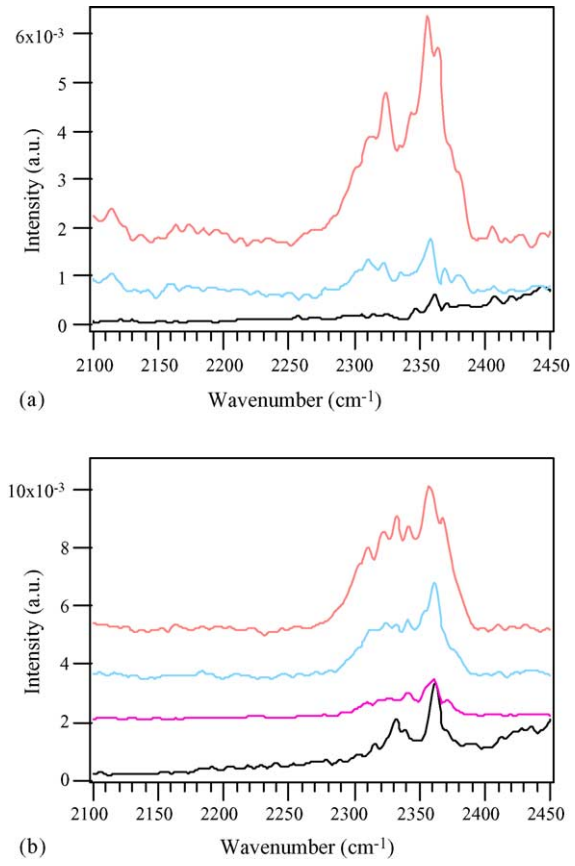

Fig. 10. DRIFT spectra obtained after exposing the $WO_3/CeO_2/YSZ$ nanocomposite to (a) methanol and to (b) methanol + water at different temperatures: (—) RT, (—) 523 K, (—) 573 K and (—) 603 K; spectral region from 2100 to 2450 cm^{-1}.

gives rise to formates and carbon dioxide at $T \geq 523$ K [10], whereas the pure oxides show a lower reactivity with respect to methanol oxidation (methanol is oxidized to formic acid and carbon dioxide when chemisorbed on tungsten oxide at $T \geq 423$ K in mixture with oxygen [19]; CeO_2 does not exhibit a significant capability in oxidation of methanol [10]).

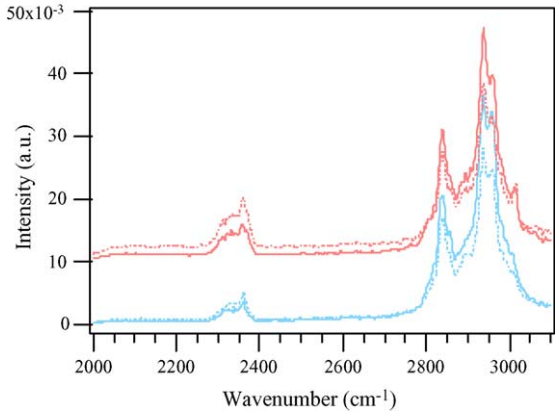

Fig. 11. DRIFT spectra obtained after exposing the $WO_3/CeO_2/YSZ$ nanocomposite to a methanol + water mixture (continuous line) and after 15 min (dotted line) at (—) 573 K and (—) 603 K; spectral region from 2000 to 3100 cm^{-1}.

The investigation of the spectra collected as a function of time (Fig. 11) suggests that the alcohol oxidation is a slow process: the signals attributed to carbon dioxide increase with exposure time, whereas the ones due to methanol (see, as an example, the C–H stretching contributions at 2780–3060 cm^{-1}) decrease.

4. Conclusions

In this paper a $WO_3/CeO_2/YSZ$ nanocomposite is prepared by wet impregnation. The supporting CeO_2/YSZ is obtained by the impregnation of a commercial YSZ powder with a solution of $Ce(NO_3)_3{\cdot}6H_2O$, whereas for the $WO_3/CeO_2/YSZ$ system an aqueous solution of ammonium metatungstate is used. The adopted nominal atomic ratios are: W/Zr = 0.025, Ce/Zr = 0.020.

XP data reveal a marked reduction of the deposited cerium and tungsten oxides: Ce(III), in particular, seems to be the prevailing species. The experimental atomic ratios allow to exclude the diffusion of the deposited oxide inside the support. Both XP and IR data are consistent with a lower hydroxylation of the $WO_3/CeO_2/YSZ$ nanocomposite surface with respect to CeO_2/YSZ. This suggests a grafting mechanism by means of hydroxyl groups.

The XRD pattern of $WO_3/CeO_2/YSZ$ reveals only the contributions of YSZ.

The acidic sites are investigated by means of the exposure to pyridine whereas carbon dioxide was preferred for basic and complex sites. As evidenced by studying the interaction with pyridine and carbon dioxide, the deposition of WO_3 strongly decreases the Lewis and Brønsted acidic and basic sites distributed on the CeO_2/YSZ surface. Consistently, the interaction of methanol is mainly molecular.

The reactivity of $WO_3/CeO_2/YSZ$ with respect to methanol is investigated in the presence and in the absence of water; in both cases the only product of methanol oxidation is carbon dioxide. Carbon dioxide forms at RT when water is present and at $T \geq 573$ K if water is absent.

It is noteworthy saying that a nitrogen flow easily removes the oxidation products suggesting that carbon dioxide does not poison the sample surface.

Acknowledgments

The Authors gratefully acknowledge Professor E. Tondello for his helpful discussions and Dr. R. Saini for Thermal Analysis measurements.

References

[1] L. Carrette, K.A. Friedrich, U. Stimming, Chem. Phys. Chem. 1 (2000) 162–193.

[2] J. Larmine, A. Dicks, Fuel Cell Systems Explained, Wiley, Chichester, 2000.
[3] N.Q. Minh, T. Takahashi, Science and Technology of Ceramic Fuel Cells, Elsevier, Amsterdam, 1995.
[4] K. Klabunde, Nanoscale Materials in Chemistry, Wiley, New York, 2001.
[5] A. Trovarelli, Catal. Rev. Sci. Eng. 38 (1996) 439–520.
[6] S. De Rossi, E. Iguchi, M. Schiavello, R.J.D. Tilley, Z. Phys. Chem. Neue Fol. 103 (1976) 193–202.
[7] M. Schiavello, F. Pepe, M. Cannizzaro, S. De Rossi, R.J.D. Tilley, Z. Phys. Chem. Neue Fol. 106 (1977) 45–56.
[8] J. Haber, J. Janas, M. Schiavello, R.J.D. Tilley, J. Catal. 82 (1983) 395–403.
[9] M.M. Natile, F. Grillo, A. Glisenti, Top. Catal., submitted for publication.
[10] M.M. Natile, A. Glisenti, in preparation.
[11] E.P. Parry, J. Catal. 2 (1963) 371–379.
[12] L.H. Little, Infrared Spectra of Adsorbed Species, Academic Press, San Diego, CA, 1966.
[13] P. Nortier, P. Fourre, A.B. Mohammed Saad, O. Saur, J.C. Lavalley, Appl. Catal. 61 (1990) 141–160.
[14] G. Busca, Catal. Today 41 (1998) 191–206.
[15] A. Auroux, A. Gervasini, J. Phys. Chem. 94 (1990) 6371–6379.
[16] D.G. Rethwisch, J.A. Dumesic, Langmuir 2 (1986) 73–79.
[17] J.C. Lavalley, Catal. Today 27 (1996) 377–401.
[18] D. Martin, D. Duprez, J. Mol. Catal. A: Chem. 118 (1997) 113–128.
[19] A. Tocchetto, A. Glisenti, Langmuir 16 (2000) 6173–6182.
[20] Nominal atomic ratio are obtained from the precursors weighed quantities.
[21] P. Kubelka, F. Munk, Z. Tech. Phys. 12 (1931) 593.
[22] G. Kortum, Reflectance Spectroscopy, Springer, New York, 1969.
[23] D.A. Shirley, Phys. Rev. B 5 (1972) 4709–4714.
[24] J.F. Moulder, W.F. Stickle, P.E. Sobol, K.D. Bomben, in: J. Chastain (Ed.), Handbook of X-ray Photoelectron Spectroscopy, Perkin-Elmer Corporation Physical Electronics Division, Eden Prairie, MN, 1992.
[25] P.W. Park, J.S. Ledford, Langmuir 12 (1996) 1794–1799.
[26] M.V. Rama Rao, T. Shripathi, J. Electron Spectrosc. Relat. Phenom. 87 (1997) 121–126.
[27] M. Fernández García, A. Martínez Arias, J.C. Hanson, J.A. Rodriguez, Chem. Rev. 104 (2004) 4063–4104.
[28] C.S. Fadley, in: C.R. Brundle, A.D. Baker (Eds.), Electron Spectroscopy: Theory, Techniques and Applications, Academic Press, London, 1978 (Chapter 1).
[29] N.S. McIntyre, T.C. Chan, in: D. Briggs, M.P. Seah (Eds.), Practical Surface Analysis, vol. 1, 2nd ed., Wiley, Chichester, 1990 (Chapter 1).
[30] C. Bigey, L. Hilaire, G. Maire, J. Catal. 198 (2001) 208–222.
[31] M.P. Rosynek, D.T. Magnuson, J. Catal. 48 (1977) 417–421.
[32] L. Corrsin, B.J. Fax, R.C. Lord, J. Chem. Phys. 21 (1953) 1170–1176.
[33] M.I. Zaki, M.A. Hasan, F.A. Al-Sagheer, L. Pasupulety, Colloids Surf. A 190 (2001) 261.
[34] M.I. Zaki, G.A.M. Hussein, S.A.A. Mansour, H.A. El-Ammawy, J. Mol. Catal. 51 (1989) 209–220.
[35] M.I. Zaki, G.A.M. Hussein, S.A.A. Mansour, H.M. Ismail, G.A.H. Mekhemer, Colloids Surf. A 127 (1997) 47–56.
[36] M. Falk, E. Whalley, J. Chem. Phys. 34 (1961) 1554–1568.
[37] G. Herzberg, Infrared and Raman Spectra of Polyatomic Molecules, Van Nostrand, New York, 1949.
[38] A. Badri, C. Binet, J.-C. Lavalley, J. Chem. Soc., Faraday Trans. 93 (1997) 1159–1168.
[39] A. Siokou, R.M. Nix, J. Phys. Chem. B 103 (1999) 6984–6997.